

UltraSam: A Foundation Model for Ultrasound using Large Open-Access Segmentation Datasets

Adrien Meyer^{a,b}, Aditya Murali^{a,b}, Didier Mutter^b, Nicolas Padoy^{a,b}

^aUniversity of Strasbourg, CNRS, INSERM, ICube, UMR7357, Strasbourg, France
^bIHU-Strasbourg, Institute of Image-Guided Surgery, Strasbourg, France

Purpose: Automated ultrasound image analysis is challenging due to anatomical complexity and limited annotated data. To tackle this, we take a data-centric approach, assembling the largest public ultrasound segmentation dataset and training a versatile visual foundation model tailored for ultrasound.

Methods: We compile US-43d, a large-scale collection of 43 open-access ultrasound datasets with 280,000+ images and segmentation masks for over 50 anatomical structures. We then introduce UltraSam, an adaptation of the Segment Anything Model (SAM) that is trained on US-43d and supports both point- and box-prompts. Finally, we introduce a new use case for SAM-style models by using UltraSam as a model initialization that can be finetuned for various downstream analysis tasks, demonstrating UltraSam’s foundational capabilities.

Results: UltraSam achieves vastly improved performance over existing SAM-style models for prompt-based segmentation on three diverse public datasets. Moreover, an UltraSam-initialized Vision Transformer surpasses ImageNet-, SAM-, and MedSAM-initialized models in various downstream segmentation and classification tasks, highlighting UltraSam’s effectiveness as a foundation model.

Conclusion: We compile US-43d, a large-scale unified ultrasound dataset, and introduce UltraSam, a powerful multi-purpose SAM-style model for ultrasound images. We release our code and pretrained models at <https://github.com/CAMMA-public/UltraSam> and invite the community to further this effort by continuing to contribute high-quality datasets.

Keywords: Foundation Models, SAM, Ultrasound, Large-Scale Dataset

1. Introduction

Ultrasound (US) has become indispensable in modern medicine thanks to its ability to provide real-time, safe, and cost-effective imaging. It plays a crucial role in dynamic assessments, such as fetal monitoring, and its portability makes it accessible even in low-resource settings, significantly enhancing the reach of diagnostic care.

Despite its benefits, ultrasound presents challenges such as noise, variability, and the need for specialized interpretation. Many deep learning solutions have been proposed, ranging from anatomical landmark identification, to tissue characterization from digital biopsy, to needle tracking during interventional procedures [1, 48], offering the potential to reduce reliance on specialized expertise. However, these methods rely on large volumes of annotated data, which are scarce and lack diversity due to the need for expert annotation. This problem is furthered by two key factors: (1) the substantial domain shift between natural and ultrasound images makes conventional finetuning challenging, and (2) the variability within ultrasound itself, as images differ greatly across examination areas (e.g. chest, ovarian, endoscopic), making it difficult to train general-purpose ultrasound models.

In general computer vision, the Segment Anything Model

(SAM) [25] has emerged as a foundational approach for interactive open-set segmentation. SAM’s key innovation lies in using instance-specific prompts, such as points or bounding boxes, rather than a pre-defined list of classes, to generate segmentation masks at varying levels of granularity. As a result, SAM can be directly trained on diverse large-scale datasets, and has demonstrated impressive zero-shot segmentation capabilities.

Still, SAM faces significant challenges in ultrasound imaging due to the complexity of ultrasound data, which differs greatly from natural images. Recent efforts such as MedSAM [29], SAM-Med [9], and Medical SAM Adapter [43] have attempted to adapt SAM for medical imaging, but they continue to struggle with ultrasound, suggesting the need for more specialized approaches. A few works have pursued this direction: SAMUS [28] introduces US30K built from seven public datasets while BUSSAM [38] adapts SAM for breast lesion segmentation; however, the former is still relatively small-scale and the model checkpoints remain private, while the latter is tailored to a specific organ and dataset. Overall, the community still lacks a general-purpose SAM-style model that can be applied out-of-the-box to diverse ultrasound data.

In this study, we fill this gap by (1) compiling US-43d, a collection of 280,000 image-segmentation mask pairs from 43 public datasets and (2) introducing UltraSam, a version of SAM fully-finetuned on US-43d. UltraSam is an extremely

¹Corresponding author: ameyer1@unistra.fr

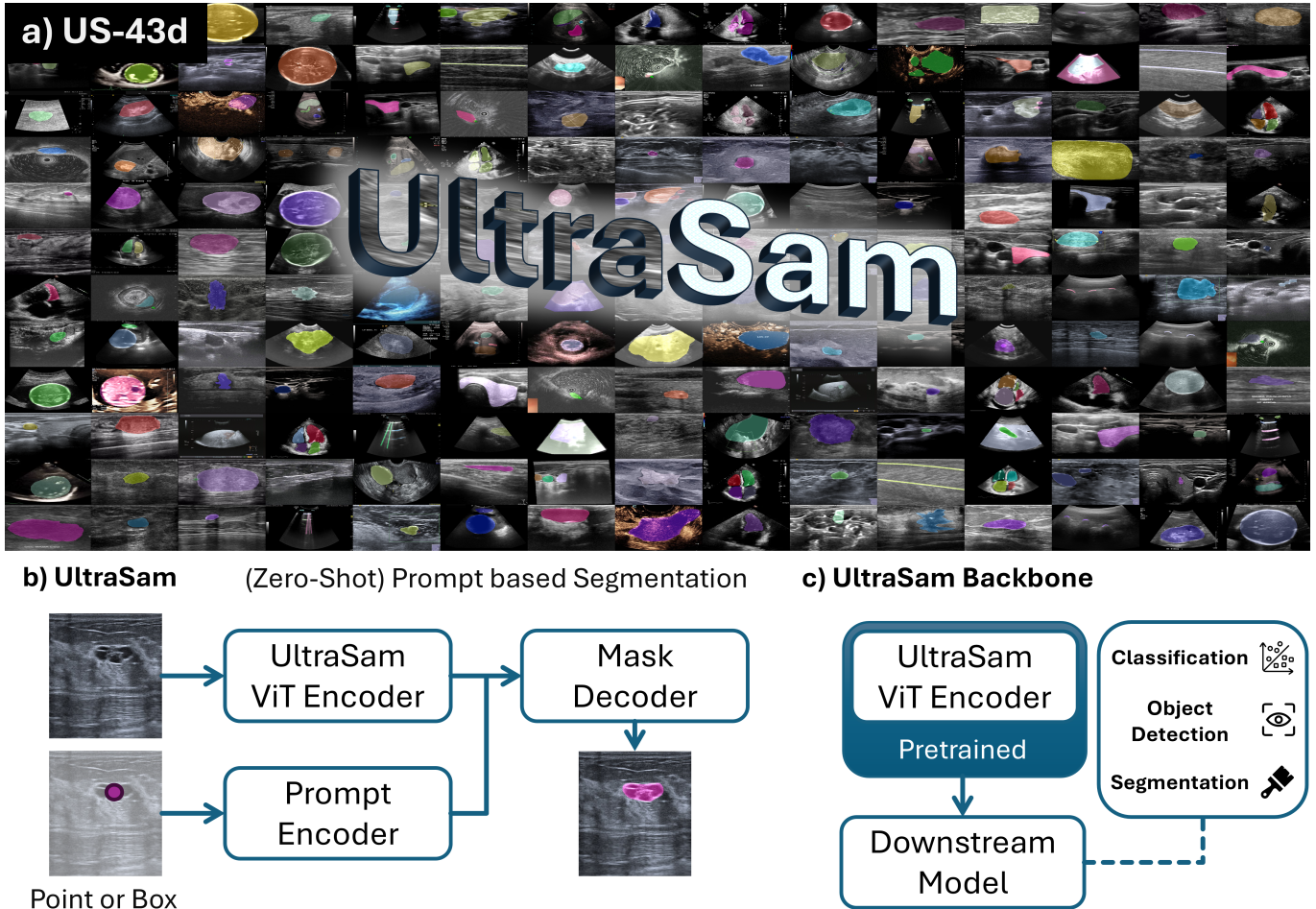


Fig. 1. UltraSam overview. a) We introduce US-43d, a large-scale open ultrasound segmentation dataset. b) Fine-tuning SAM on US-43d enables strong zero-shot, prompt-based segmentation. c) UltraSam’s pretrained feature extractor provides a robust foundation for downstream tasks like classification and segmentation.

powerful interactive segmentation model and achieves strong performance even on completely unseen organs. Moreover, because we fully finetune SAM, we also explore a new use case for SAM-style models, using UltraSam as a backbone weight initialization to boost performance on various downstream tasks. Our contributions are threefold:

1. We compile and release the largest publicly available collection of ultrasound segmentation data, US-43d, consisting of 43 datasets and 280,000 pairs of images and masks, covering 20 different clinical applications.
2. We introduce and release UltraSam, an ultrasound-adapted version of SAM.
3. We demonstrate the effectiveness of UltraSam for (zero-shot) interactive segmentation, instance segmentation, and image classification tasks.

2. Methodology

2.1. Dataset

Ultrasound imaging presents a substantial domain gap compared to other medical imaging modalities; building an

ultrasound-specific foundation model therefore requires a specialized large-scale dataset. To build such a dataset, we crawled a multitude of platforms for ultrasound data: Papers with Code, Google Dataset Search, GitHub, Google Scholar, Kaggle, ResearchGate, Mendeley dataset, Zenodo and Data in Brief. Through this process, we arrived at US-43d (see Fig. 1.a), a collection of 43 datasets covering 20 different clinical applications, containing over 280,000 annotated segmentation masks from both 2D and 3D scans [1, 44, 27, 2, 36, 32, 6, 30, 24, 49, 15, 14, 23, 39, 45, 13, 11, 48, 5, 42, 31, 20, 19, 12, 10, 22, 47, 3, 34, 21, 18, 37, 40, 33, 4, 16, 46, 17, 41, 35, 26]. US-43d captures organ and lesion of various shapes, sizes, and textures across clinical applications such as cardiac, fetal head, thyroid, and breast lesions, providing a comprehensive view of the medical ultrasound landscape (see Fig. 2). We detail the individual datasets comprising US-43d in the supplementary material.

For testing, we select three diverse datasets: BUS-BRA [13] (breast lesions), MMOTU2D [48] (ovarian lesions), and GIST514-DB [18] (gastrointestinal stromal tumors). Together they include linear and radial probes, endoscopic and non-endoscopic ultrasound, and encompass various clinical appli-

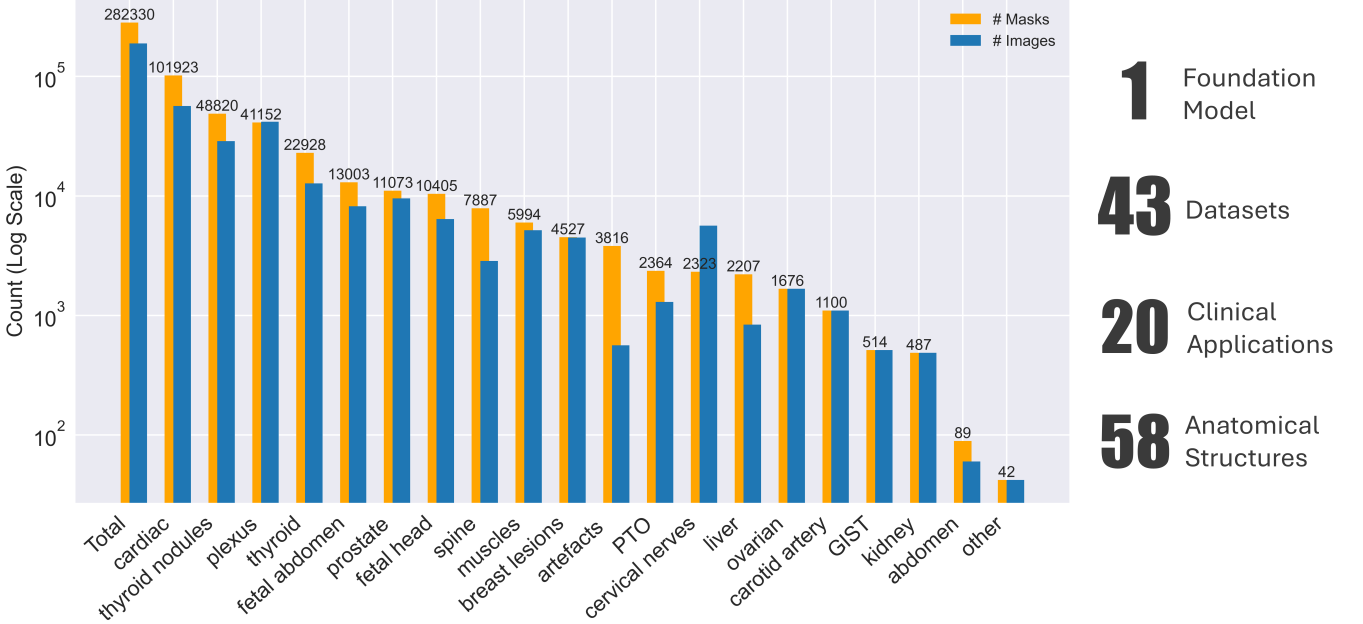


Fig. 2. Overview of US-43d, grouped by clinical applications.

cations, anatomical regions, lesion types, and imaging techniques, enabling exhaustive evaluation of UltraSam’s generalizability. We use their official test sets. We allocate 5% of each of the US-43d dataset for validation and use the remaining 95% for training. We preprocess all images to remove label-background overlaps (common in 3D ultrasound), and use the sagittal view in 3D images. We also provide scripts to convert the 43 datasets into the widely used COCO format.

BUS-BRA. The BUS-BRA [13] dataset contains 1875 breast lesion images from 1064 female patients, acquired using four ultrasound scanners at the National Institute of Cancer (Rio de Janeiro, Brazil). Breast lesion analysis in ultrasound images is well-explored, providing an ideal context for studying the capabilities of our approach.

MMOTU2D. The MMOTU2D [48] dataset contains 1469 2D ultrasound images of ovarian tumors from 247 patients, acquired at Beijing Shijitan Hospital, China. As it covers 8 different lesion types, it can also serve as a classification benchmark.

GIST514-DB. GIST514-DB [18] is an endoscopic ultrasound dataset containing a total of 514 cases, divided into 251 gastrointestinal stromal tumor (GIST) cases and 263 leiomyoma cases. Unlike other datasets in the US-43d collection, GIST514-DB features a full radial probe view, which substantially alters the image appearance.

2.2. UltraSam

We adopt the architecture of SAM [25], depicted in Fig. 1.b, which utilizes a Vision Transformer (ViT) encoder to extract image features as tokens. A prompt encoder transforms prompts (such as points or boxes) into object query tokens. These tokens interact with the image feature tokens through a transformer decoder, enabling reasoning and interaction between prompts and vision tokens. A mask head predicts mul-

iple mask outputs, each with a corresponding predicted Intersection over Union (IoU) score, allowing selection of the best predicted mask. In an additional pass through the decoder, the mask logits from the previous iteration are encoded and added element-wise to the image embedding, refining the mask prediction.

During training, we simulate user prompts by randomly sampling either a point or a box with equal probability for each instance. The point is selected randomly within the instance mask, while the box is a noised version of the ground truth box annotation. To generate this noise, the two box corners are randomly displaced by up to 5 percents of the box’s width and height. For evaluation, we follow SAM’s approach and report results using either the center point or the ground truth box as prompt.

We also evaluate UltraSam for downstream tasks (see Fig. 1.c), leveraging its feature extractor as a pretrained backbone for our models.

Implementation details. UltraSam was trained using the pretrained SAM ViT-b model on four H100 GPUs for 16 hours, with a batch size of eight images per GPU. The images were resized so their longest side was 1024 pixels, with random horizontal flips applied. The implementation utilized the MMDetection v3.3 library [7]. The model was fine-tuned for 30,000 iterations, with the learning rate reduced by a factor of 10 at the 20,000th and 28,888th iterations. We used the AdamW optimizer, starting with an initial learning rate of 1×10^{-4} and a warm-up period of 500 iterations. We use a combination of focal and dice loss for segmentation, and L1 loss for IoU prediction.

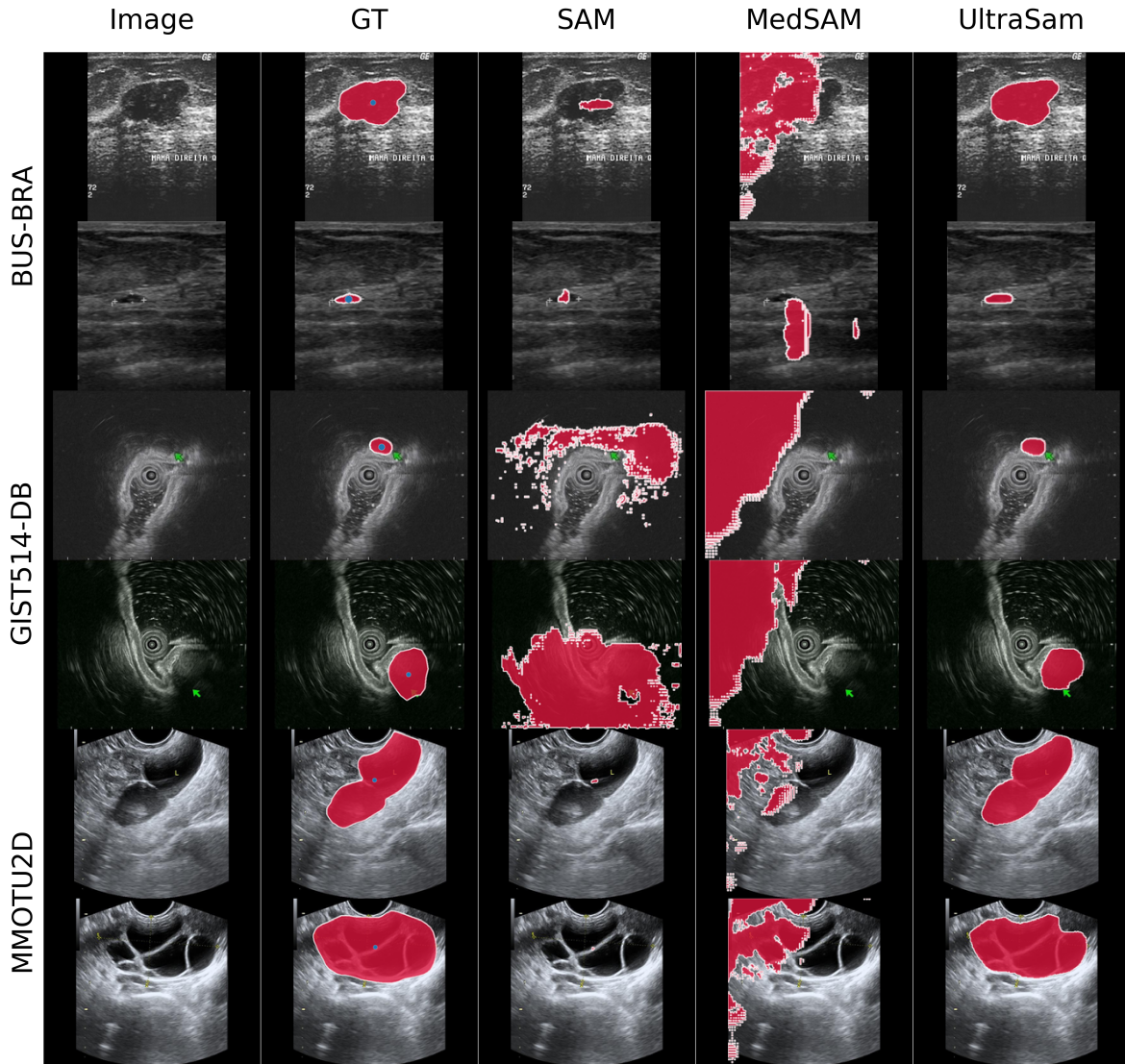


Fig. 3. Qualitative results for interactive segmentation with a single point-prompt.

3. Evaluation

3.1. Interactive Segmentation

We evaluate UltraSam for prompt-based segmentation using either the ground-truth center point or bounding box as prompts. We compare to the original SAM and its medical adaptation, MedSAM. Then, to explore performance on unseen organs and target structures, we train a variant of UltraSam for each test dataset, excluding any training data containing the targeted organ². We denote these variants UltraSam*.

3.2. Downstream task evaluation

In addition to enabling prompt-based segmentation, UltraSam’s feature extractor serves as a powerful pretrained ViT

for ultrasound. To evaluate its capabilities, we test it on two downstream tasks: instance segmentation and image classification.

Instance Segmentation. We use the state-of-the-art Mask2Former [8] as our instance segmentation model, replacing its Resnet backbone with UltraSam’s ViT. We compare its performance against SAM and MedSAM’s ViT backbones, as well as the ImageNet-pretrained Resnet-50. The Mask2Former decoder is randomly initialized. We use the default hyperparameters of [7] and train the models for 8,000 iterations with a batch size of 8 on a single A100 GPU.

Image Classification. For image classification, we build a simple classifier using UltraSam’s ViT as the model backbone. We average the output tokens and apply a linear classifier to predict the label. We compare this approach against SAM and MedSAM’s ViT initialization as well as to an ImageNet-pretrained Resnet-50. We train all models using focal loss to address data imbalance.

²During training, UltraSam*-BUSBRA excludes all breast US images, UltraSam*-MMOTU2D excludes all ovarian US, and UltraSam*-GIST514DB excludes all gastrointestinal US.

Table 1. Interactive segmentation results (mAP, %). Evaluated using either the center point of the ground truth (gt) mask or the gt box as prompts. UltraSam* denotes zero-shot performance. Bold indicates best performance.

Models	Prompt	BUS-BRA		MMOTU2D		GIST514-DB	
		mAP	mAP@50	mAP	mAP@50	mAP	mAP@50
SAM	Point	14.2	27.2	2.1	4.7	6.2	12.2
MedSAM		0.0	0.0	0.0	0.0	0.0	0.0
UltraSam		67.5	95.7	57.5	85.7	55.5	90.8
UltraSam*		58.3	92.7	44.4	70.6	9.3	17.4
SAM	Box	68.1	100	34.5	58.8	57.2	92.2
MedSAM		59.1	98.9	48.8	95.4	30.4	81.0
UltraSam		79.1	99.0	79.5	100	73.0	100
UltraSam*		76.5	100	79.6	100	69.4	98.9

Table 2. Image classification results: Precision (Prec), Recall, and F1-score (%). Backbones are varied to demonstrate transfer learning effectiveness. Resnet-50 is initialized with ImageNet weights. Bold indicates best performance.

Backbones	BUS-BRA			MMOTU2D			GIST514-DB		
	prec	recall	f1	prec	recall	f1	prec	recall	f1
Resnet-50	72.1	70.2	70.9	40.6	40.5	38.4	83.4	82.3	81.9
SAM	80.1	78.3	79.1	52.3	51.6	51.2	86.7	85.1	84.8
MedSAM	84.9	82.9	83.8	57.9	50.6	52.2	72.4	70.1	69.1
UltraSam	87.6	87.5	87.5	62.6	62.4	62.0	78.2	74.2	73.5

4. Experiments

4.1. Interactive Segmentation

We present the prompt-based segmentation results in Table 1, using either the instance’s center point or bounding box as prompts. Following classical instance segmentation work, we report mean Average Precision (mAP), which measures precision across multiple IoU thresholds (0.5 to 0.95), and mAP@50, which measures precision at a fixed IoU threshold of 50%.

When using point prompts, UltraSam substantially outperforms all baselines, achieving mAP scores of 67.5, 57.5, and 55.5 for BUS-BRA, MMOTU2D, and GIST514-DB, respectively. SAM struggles with ultrasound structures due to domain shifts in its training data, while MedSAM, lacking point prompt training, fails completely in this setting. UltraSam* also demonstrates strong zero-shot performance, except on the GIST514-DB dataset. This can be explained by the fact that GIST514-DB contains full radial views, which differ from the rest of the US-43d data, affecting performance. These trends are illustrated qualitatively in Fig. 3 (more results in the supplementary material), where UltraSam consistently identifies structures that SAM and MedSAM fail to segment.

With box prompts, SAM and MedSAM improve greatly but still fall behind UltraSam and UltraSam*. UltraSam achieves near-perfect mAP@50 scores (99, 100, and 100 for BUS-BRA, MMOTU2D, and GIST514-DB) and strong mAP results (79.1, 79.5, and 73.0, respectively).

4.2. Instance Segmentation

We present the instance segmentation results in Table 3, reporting mAP and mAP@50 for both object detection and in-

stance segmentation. Finetuning the UltraSam backbone leads to a substantial gain of 3-5% mAP on the BUS-BRA and MMOTU2D datasets. However, on GIST514-DB, as with the prompt-based segmentation, directly finetuning SAM outperforms all models. Notably, UltraSam still outperforms MedSAM on GIST514-DB, showing that specialized ultrasound finetuning is still effective but could be further improved by increased data diversity in the training set.

4.3. Image Classification

We present the image classification results in Table 2, reporting precision, recall, and F1-score (%). Once again, UltraSam outperforms all other methods on the BUS-BRA and MMOTU2D datasets by a comfortable margin but falls behind SAM on the GIST514-DB dataset. UltraSam improve upon SAM by +8.4 and +10.8 f1-score (%) on BUS-BRA and MMOTU2D, respectively.

Table 3. Instance segmentation and object detection results (mAP, %), using Mask2Former [8]. Backbones are varied to show transfer learning effectiveness. Resnet-50 is initialized with ImageNet weights. Bold indicates best performance.

Datasets	Backbones	Detection		Segmentation	
		mAP	mAP@50	mAP	mAP@50
BUS-BRA	Resnet-50	60.1	84.3	59.0	83.5
	SAM	55.2	77.2	54.7	78.0
	MedSAM	58.7	83.4	57.4	84.2
	UltraSam	60.7	86.0	60.9	87.2
MMOTU2D	Resnet-50	19.1	27.4	18.9	27.4
	SAM	19.6	28.8	19.3	28.9
	MedSAM	18.2	27.3	18.2	28.1
	UltraSam	23.5	33.9	23.5	34.2
GIST514-DB	Resnet-50	36.2	56.8	37.3	60.5
	SAM	43.5	66.2	44.0	61.5
	MedSAM	34.3	55.0	34.8	53.7
	UltraSam	37.8	59.0	38.4	58.0

5. Discussion and Conclusion

UltraSam, with its dedicated US-43d dataset, demonstrates impressive prompt-based segmentation capabilities, excelling even in zero-shot settings. Its ViT-encoder proves to be a robust pretrained initialization for downstream tasks, consistently outperforming other SAM-based models and ImageNet initialization on BUS-BRA and MMOTU2D evaluations for both classification and segmentation. These results highlight the power of domain-specific fine-tuning, where UltraSam surpasses both SAM and MedSAM. Additionally, UltraSam’s efficiency in segmentation makes it a valuable tool for accelerating annotation processes.

However, UltraSam’s performance declines on datasets that differ significantly from US-43d, where it underperforms compared to SAM on downstream tasks. This highlights the

need to expand US-43d for greater generalizability. We encourage the research community to contribute additional high-quality ultrasound datasets, especially in underrepresented areas, to improve the model's adaptability across diverse applications. With the release of US-43d, the pretrained UltraSam checkpoint, and our code, we hope to provide valuable resources that advance future research in the field.

6. Acknowledgement

This research was conducted within the framework of the APEUS, supported by the ARC Foundation (www.fondation-arc.org). This work was also partially supported by French state funds managed within the National AI Chair program under Grant ANR-20-CHIA0029-01 (Chair AI4ORSafety) and within the 'Plan Investissements d'Avenir', funded by the ANR (reference ANR-10-IAHU-02).

Ethical Approval: This article does not contain any studies with human participants or animals performed by any of the authors.

Competing Interests: The authors declare no conflict of interest.

Informed Consent: This manuscript does not contain any patient data.

References

- [1] (2024) Nerve block target localization and needle guidance for autonomous robotic ultrasound guided regional anesthesia, URL https://github.com/Regional-US/brachial_plexus, accessed: 10/18/2024, Submitted to IROS-2024
- [2] AIMI S (2021) Thyroid ultrasound cine-clip. URL <https://stanfordaimi.azurewebsites.net/datasets/a72f2b02-7b53-4c5d-963c-d7253220bfd5>, accessed: 10/18/2024
- [3] Al-Dhabyani W, Gomaa M, Khaled H, et al (2020) Dataset of breast ultrasound images. *Data in brief* 28:104863
- [4] Ardakani AA, Mohammadi A, Mirza-Aghazadeh-Attari M, et al (2023) An open-access breast lesion ultrasound image database: Applicable in artificial intelligence studies. *Computers in Biology and Medicine* 152:106438
- [5] Ashkani Chenarlogh V, Ghelich Oghli M, Shabanzadeh A, et al (2022) Fast and accurate u-net model for fetal ultrasound image segmentation. *Ultrasonic imaging* 44(1):25–38
- [6] Baum ZMC, Saeed SU, Min Z, et al (2023) MR to Ultrasound Registration for Prostate Challenge - Dataset. <https://doi.org/10.5281/zenodo.8004388>
- [7] Chen K, Wang J, et al (2019) Mmdetection: Open mmlab detection toolbox and benchmark. arXiv preprint arXiv:190607155
- [8] Cheng B, Misra I, et al (2021) Masked-attention mask transformer for universal image segmentation. arXiv
- [9] Cheng J, Ye J, Deng Z, et al (2023) Sam-med2d. 2308.16184
- [10] Cunningham R, Sánchez MB, May G, et al (2018) Estimating full regional skeletal muscle fibre orientation from b-mode ultrasound images using convolutional, residual, and deconvolutional neural networks. *Journal of Imaging* 4(2):29
- [11] Da Correggio KS, Noya Galluzzo R, Santos LO, et al (2023) Fetal abdominal structures segmentation dataset using ultrasonic images. <https://doi.org/10.17632/4gcpm9dsc3.1>
- [12] Ding Y, Member I, Yang Q, et al (2022) Mallesnet: A multi-object assistance based network for brachial plexus segmentation in ultrasound images. *Medical Image Analysis* 80:102511
- [13] Gómez-Flores W, et al (2024) Bus-bra: A breast ultrasound dataset for assessing computer-aided diagnosis systems. *Medical Physics* 51(4):3110–3123
- [14] Gong H, Chen G, et al (2021) Multi-task learning for thyroid nodule segmentation with thyroid region prior. In: 2021 IEEE 18th international symposium on biomedical imaging (ISBI), IEEE, pp 257–261
- [15] Gong H, Chen J, et al (2023) Thyroid region prior guided attention for ultrasound segmentation of thyroid nodules. *Computers in biology and medicine* 155:106389
- [16] Guo Y, Duan X, Wang C, et al (2021) Segmentation and recognition of breast ultrasound images based on an expanded u-net. *Plos one* 16(6):e0253202
- [17] Hann A, Bettac L, Haenle MM, et al (2017) Algorithm guided outlining of 105 pancreatic cancer liver metastases in ultrasound. *Scientific Reports* 7(1):12779. <https://doi.org/10.1038/s41598-017-12829-5>
- [18] He Q, Bano S, Liu J, et al (2023) Query2: Query over queries for improving gastrointestinal stromal tumour detection in an endoscopic ultrasound. *Computers in Biology and Medicine* 152:106424
- [19] van den Heuvel T, de Bruijn D, de Korte CL, et al (2018) Automated measurement of fetal head circumference. <https://doi.org/10.5281/zenodo.1322001>
- [20] van den Heuvel TL, de Bruijn D, de Korte CL, et al (2018) Automated measurement of fetal head circumference using 2d ultrasound images. *PloS one* 13(8):e0200412
- [21] Howell L, Ingram N, Lapham R, et al (2024) Deep learning for real-time multi-class segmentation of artefacts in lung ultrasound. *Ultrasonics* 140:107251
- [22] Iqbal A, Sharif M (2024) Memory-efficient transformer network with feature fusion for breast tumor segmentation and classification task. *Engineering Applications of Artificial Intelligence* 127:107292
- [23] Jiang H, Imran M, et al (2024) Microsegnet: A deep learning approach for prostate segmentation on micro-ultrasound images. *Computerized Medical Imaging and Graphics* 112:102326
- [24] Jieyun B, ZhanHong O (2024) Pubic Symphysis-Fetal Head Segmentation and Angle of Progression. <https://doi.org/10.5281/zenodo.10829116>
- [25] Kirillov A, et al (2023) Segment anything. In: Proceedings of the IEEE/CVF International Conference on Computer Vision, pp 4015–4026
- [26] Krönke M, Eilers C, Dimova D, et al (2022) Tracked 3d ultrasound and deep neural network-based thyroid segmentation reduce interobserver variability in thyroid volumetry. *PLOS ONE* 17(7):e0268550. <https://doi.org/10.1371/journal.pone.0268550>
- [27] Leclerc S, Smistad E, et al (2019) Deep learning for segmentation using an open large-scale dataset in 2d echocardiography. *IEEE transactions on medical imaging* 38(9):2198–2210
- [28] Lin X, Xiang Y, Zhang L, et al (2023) Samus: Adapting segment anything model for clinically-friendly and generalizable ultrasound image segmentation. 2309.06824
- [29] Ma J, He Y, et al (2024) Segment anything in medical images. *Nature Communications* 15(1):654
- [30] Marzola F, van Alfen N, et al (2021) Dataset for "deep learning segmentation of transverse musculoskeletal ultrasound images for neuromuscular disease assessment". <https://doi.org/10.17632/3jy kz7wz8d.1>
- [31] Momot A (2022) Common carotid artery ultrasound images. <https://doi.org/10.17632/d4xt63mgjm.1>
- [32] Montoya A, Hasnin, et al (2016) Ultrasound nerve segmentation. URL <https://kaggle.com/competitions/ultrasound-nerve-segmentation>, kaggle competition
- [33] Pawłowska A, Ćwierz-Pieńkowska A, Domalik A, et al (2024) Curated benchmark dataset for ultrasound based breast lesion analysis. *Scientific Data* 11(1):148
- [34] Pedraza L, Vargas C, Narváez F, et al (2015) An open access thyroid ultrasound image database. In: 10th International symposium on medical information processing and analysis, SPIE, pp 188–193
- [35] Reddy CD, Lopez L, Ouyang D, et al (2023) Video-based deep learning for automated assessment of left ventricular ejection fraction in pediatric patients. *Journal of the American Society of Echocardiography* 36(5):482–489. <https://doi.org/10.1016/j.echo.2022.12.008>
- [36] Sappia MS, Murphy K, et al (2024) Abdominal circumference operator-agnostic ultrasound measurement in low-income countries using artificial intelligence. <https://doi.org/10.5281/zenodo.10991270>

- [37] Singla R, Ringstrom C, Hu G, et al (2023) The open kidney ultrasound data set. In: International Workshop on Advances in Simplifying Medical Ultrasound, Springer, pp 155–164
- [38] Tu Z, et al (2024) Ultrasound sam adapter: Adapting sam for breast lesion segmentation in ultrasound images. arXiv preprint arXiv:240414837 URL <https://arxiv.org/abs/2404.14837>
- [39] Ungi T, Greer H, et al (2020) Automatic spine ultrasound segmentation for scoliosis visualization and measurement. *IEEE Transactions on Biomedical Engineering* 67(11):3234–3241
- [40] Vallez N, Bueno G, Deniz O, et al (2024) Bus-uclm: Breast ultrasound lesion segmentation dataset. <https://doi.org/10.17632/7fvgj4j5p7.1>
- [41] Vitale S, Orlando JI, Iarussi E, et al (2020) Improving realism in patient-specific abdominal ultrasound simulation using cyclegans. *International Journal of Computer Assisted Radiology and Surgery* 15(2):183–192. <https://doi.org/10.1007/s11548-019-02068-5>
- [42] Wang T, Li Z, Huang M, et al (2021) Echocp: An echocardiography dataset in contrast transthoracic echocardiography for patent foramen ovale diagnosis. In: *Medical Image Computing and Computer Assisted Intervention–MICCAI 2021: 24th International Conference, Strasbourg, France, September 27–October 1, 2021, Proceedings, Part VI 24*, Springer, pp 506–515
- [43] Wu J, Ji W, Liu Y, et al (2023) Medical sam adapter: Adapting segment anything model for medical image segmentation. arXiv preprint arXiv:230412620
- [44] xbhk (2024) Stu-hospital. URL <https://github.com/xbhk/STU-Hospital>, accessed: 10/18/2024
- [45] Yang J, Ding X, et al (2023) Graphecho: Graph-driven unsupervised domain adaptation for echocardiogram video segmentation. In: *Proceedings of the IEEE/CVF International Conference on Computer Vision*, pp 11878–11887
- [46] Yap MH, Pons G, Marti J, et al (2017) Automated breast ultrasound lesions detection using convolutional neural networks. *IEEE Journal of Biomedical and Health Informatics* 22(4):1218–1226. <https://doi.org/10.1109/JBHI.2017.2731873>
- [47] Yiming X, Bowen Z, Xiaohong L, et al (2022) Annotated ultrasound liver images. <https://doi.org/10.5281/zenodo.7272660>
- [48] Zhao Q, Lyu S, Bai W, et al (2022) A multi-modality ovarian tumor ultrasound image dataset for unsupervised cross-domain semantic segmentation. *CoRR* abs/2207.06799
- [49] Zhou J, Jia X, et al (2020) Thyroid Nodule Segmentation and Classification in Ultrasound Images. <https://doi.org/10.5281/zenodo.3715942>